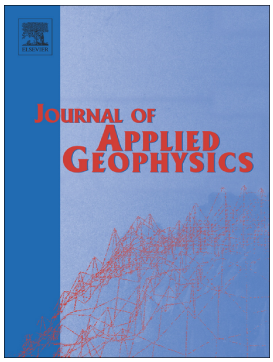

A novel approach to reduce environmental noise in microgravity measurements using a Scintrex CG5

Daniel Boddice, Phillip Atkins, Anthony Rodgers, Nicole Metje, Yuriy Goncharenko, David Chapman

PII: S0926-9851(17)30215-X
DOI: doi:10.1016/j.jappgeo.2018.03.022
Reference: APPGEO 3480

To appear in:

Received date: 2 March 2017
Revised date: 16 January 2018
Accepted date: 25 March 2018

Please cite this article as: Daniel Boddice, Phillip Atkins, Anthony Rodgers, Nicole Metje, Yuriy Goncharenko, David Chapman , A novel approach to reduce environmental noise in microgravity measurements using a Scintrex CG5. The address for the corresponding author was captured as affiliation for all authors. Please check if appropriate. Appgeo(2017), doi:10.1016/j.jappgeo.2018.03.022

A novel approach to reduce environmental noise in microgravity measurements using a Scintrex CG5

Daniel Boddice[1*], Phillip Atkins[1], Anthony Rodgers[1], Nicole Metje[1], Yuriy Goncharenko[2], David Chapman[1]

1. School of Engineering, College of Engineering and Physical Sciences, University of Birmingham, Edgbaston, Birmingham, B15 2TT
2. Microwave Systems Laboratory, Dept. of Electrical and Computer Engineering, Colorado State University, Fort Collins, CO 80523, USA (formerly of 1)

* d.boddice@bham.ac.uk

Abstract

The accuracy and repeatability of microgravity measurements for surveying purposes are affected by two main sources of noise; instrument noise from the sensor and electronics and environmental sources of noise from anthropogenic activity, wind, microseismic activity and other sources of vibrational noise. There is little information in the literature on the quantitative values of these different noise sources and their significance for microgravity measurements. Experiments were conducted to quantify these sources of noise with multiple instruments and to develop methodologies to reduce these unwanted signals thereby improving the accuracy or speed of microgravity measurements. External environmental sources of noise were found to be concentrated at higher frequencies (> 0.1 Hz), well within the instrument's bandwidth. In contrast, the internal instrumental noise was dominant at frequencies much lower than the reciprocal of the maximum integration time, and was identified as the limiting factor for current instruments. The optimum time for integration was found to be between 120 to 150 seconds for the instruments tested.

In order to reduce the effects of external environmental noise on microgravity measurements, a filtering and despiking technique was created using data from noisy environments next to a main road and outside on a windy day. The technique showed a significant improvement in

the repeatability of measurements, with between 40% and 50% lower standard deviations being obtained over numerous different data sets.

The filtering technique was then tested in field conditions by using an anomaly of known size, and a comparison made between different filtering methods. Results showed improvements with the proposed method performing better than a conventional, or boxcar, averaging process. The proposed despiking process was generally found to be ineffective, with greater gains obtained when complete measurement records were discarded. Field survey results were worse than static measurement results, possibly due to the actions of moving the Scintrex during the survey which caused instability and elastic relaxation in the sensor, or the liquid tilt sensors, which generated additional low frequency instrument noise. However, the technique will result in significant improvements to accuracy and a reduction of measurement time, both for static measurements, for example at reference sites and observatories, and for field measurements using the next generation of instruments based on new technology, such as atom interferometry, resulting in time and cost savings.

Keywords: microgravity, signal processing, noise reduction

Introduction

Microgravity measurements are a useful tool within the geophysicist's toolbox for locating subsurface voids, as the instrument responds to the physical property that defines a void as opposed to a proxy (i.e. density contrast). Furthermore, as a passive method, it measures a gravity field and thus has no theoretical limitations on penetration depth. These advantages give it a capability unparalleled by other geophysical techniques, especially for deeper features. Instruments such as the Scintrex CG5 [1] perform many corrections to the raw gravity signal for time-varying effects automatically (e.g. temperature, tilt, tide and drift) and standard data processing usually consists of data reduction of the acquired points to correct for variations in the topography and position of the gravity stations using well-understood techniques [2-6]. However, gravimeters are strongly affected during measurements by noise, defined as any unwanted signal manifesting itself in the measurements. Noise stems from both the instrument itself and from vibrational environmental sources which greatly affect the accuracy and repeatability of estimated gravity values and must be accounted for by using long integration times (i.e. the time for a single measurement cycle should be at least 30 seconds) for each measurement. Whilst the majority of surveys are to assess regional gravity fields, setup gravity networks [e.g. 7, 8-10] or locate large targets like ore bodies [e.g. 4, 11], there is a growing demand for smaller scale surveys capable of finding smaller targets in advance of civil engineering development work [e.g. 12] such as low-density ground, sinkholes and solution features. However, as the signal from these targets is notably smaller, and the sampling density reasonably coarse in relation to their size, it is imperative that data is obtained and corrected with the highest possible accuracy to avoid the creation of correlated noise signals of a similar spatial wavelength to signals from potential targets, which may result in the signal being lost in the noise or false features being detected, especially as interpolation between points is used on the final gravity map. Whilst the acquisition of high accuracy data is

important with any geophysical method, the long acquisition time for microgravity data leads to large costs involved in reacquisition of points and a lower spatial resolution than other geophysical methods making the acquisition of good quality measurements first time all the more important.

Several authors have taken long period measurements using multiple field gravimeters (CG3 and CG3M) to assess their long-term stability [e.g. 13, 14, 15] for monitoring purposes. Many of these studies were important for developing corrections for low frequency noise sources which affect measurement values between points including celestial and ocean tidal loading and atmospheric pressure changes. Extensive testing has been also been carried out on known instrumental effects such as tilt [16, 17] and temperature [14], although quantification of sensor and instrument electronic effects on the final measurement has only been defined as a general residual once all other corrections have been implemented [18].

Much less consideration has been given to higher frequency sources of noise such as wind, vibrations due to traffic and other anthropogenic activity and ambient microseism noise caused by pressure changes on the ocean floor due to the action of waves in the open ocean [19]. This is partially due to the high frequency nature of these noise sources and the resolution limitations of the CG3's 1 Hz sampling rate in comparison to the CG5 which samples at 6 Hz, although Debeglia and Dupoint [13] did note the need for statistical despiking techniques to remove statistically outlying individual samples within the signal processing. These noise sources are often accounted for in large-scale surveys by positioning measurement points away from trouble spots, such as soft ground or near to roads [5]. However, this is rarely realistic on smaller scale sites and a more practical solution is increasing the instrument's integration time to allow the noise to be averaged out using a boxcar filtering approach [13]. However, as ambient microseism noise is formed from a superposition of

primary and secondary microseisms [20] and other forms of vibrational noise such as road noise form unequal positive and negative contributions (Figure 1), the integration method is imperfect as the partially deterministic signal causes a mean shift when not integrated over infinite time. Nevertheless, integration has been shown to give accuracies of up to 5 µGal with comparatively lengthy occupations of 15-20 minutes per point [21] which are commercially unviable due to financial and time constraints. Another approach taken by Sugihara [22] is to use visual inspection of the raw data to find periods of high microseismic and wind activity and remove them from the data. Two main problems exist with this method; first it is time consuming and not necessarily statistically rigorous on large datasets and secondly, the method does not provide a clear on-site assessment of when a suitable amount of data has been collected to give sufficient accuracy. Another method is to address the noise through the use of filtering techniques such as Scintrex's own seismic filter embedded in the CG5's software, which reduces noise from microseismic wave noise and rejects spikes [1], but the operation of this filter is unknown making replication impossible from the description in the manual and no published assessment of the filter in controlled field conditions can be found to assess its effectiveness. It is therefore recognised that filtering of these higher frequency sources of noise may significantly reduce the integration times, saving time and money during a survey. This paper focuses on the quantification of these noise sources which affect the data quality of single-point measurements and some novel methods for improving data processing using the raw data from the instrument and filtering techniques. This is particularly important with the development of gravity instruments based on atom interferometry which will have an increased sensitivity to both the signal-of-interest and the unwanted noise.

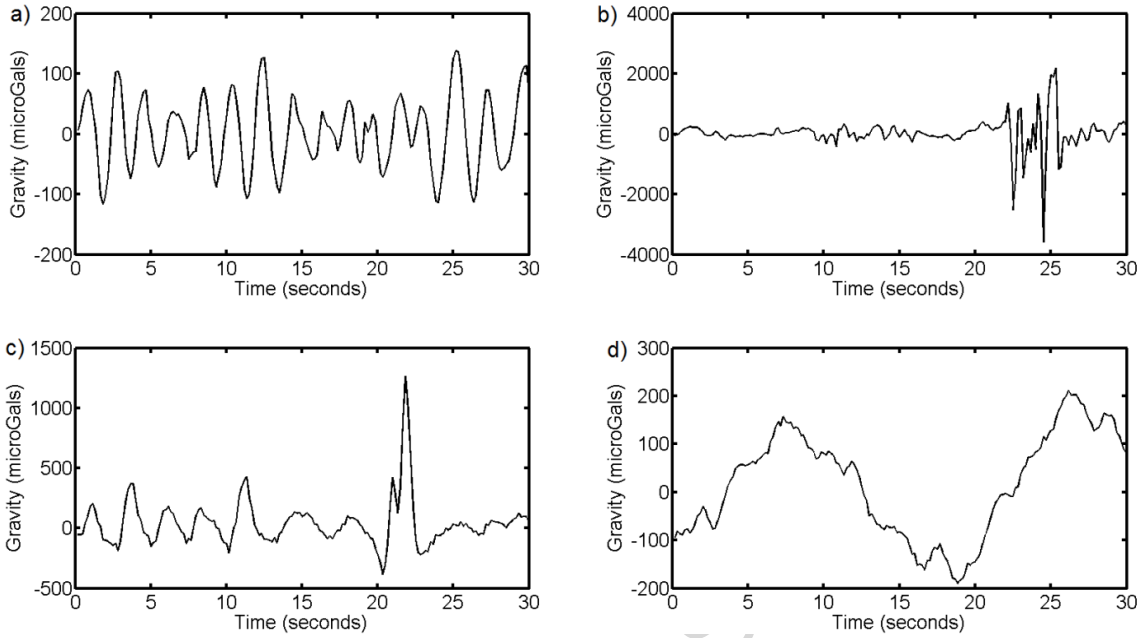

Figure 1: 30 second sections of longer gravity measurements showing the effect of measurement high-frequency noise. Notice the imbalance in positive and negative fluctuations around the mean (defined as zero). a) Microseism noise only b) microseism and wind noise spikes with negative spikes c) microseism and road traffic noise with positive spikes d) microseism and earthquake noise introducing a low-frequency signal which dominates the microseism noise

Characterisation of Noise Sources

The noise sources affecting the accuracy of a single microgravity measurement stem from two main sources; real environmental signals such as wind vibration, anthropogenic vibrational noise and microseism noise [19] which are visible regardless of the gravimeter used, and instrument specific sources of noise stemming from the instrument's electronics and sensor mechanics and which vary between gravimeters, even those of the same manufacturer and model. A summary of these sources of noise is provided in Table 1, including an approximate frequency and scale as well as a summary of the methods currently available to correct the measurements.

Table 1: Summary of the main sources of instrumental and environmental noise affecting the accuracy of individual measurements, their frequencies, size and correction methods

	Noise	Varies as a function of	Approximate Frequency	Size of error	Correction
INSTRUMENTAL NOISE	Linear creep on sensor springs	Time, Instrument	DC	Varies between instruments but < 2 mGal per day	Linear trend removal from repeat measurements over time at base station.
	Unspecified instrument noise from sensor/electronics	Time, Instrument	Lower than minimum instrument spectral resolution (< $4x10^{-3}$ Hz) of Scintrex CG5	Causes the measurement to vary ±2-8 µGal depending on the instrument even after all corrections have been applied	Can't be corrected other than by averaging multiple measurement cycles per spatial point. Represents the theoretical maximum resolution of the instrument
ENVIRONMENTAL NOISE	Ocean Tidal Loading	Time, Geographic Location	Approximately $1x10^{-5}$ Hz (one cycle per 27 hours)	In Birmingham, UK, the residual tide after high accuracy body tide model is approximately ±5-10 µGal depending on the day.	Ocean Tide models, Direct measurements, removal of a higher order drift function with frequent visits to base stations.
	Seismic noise (ocean waves and earthquakes)	Time, Geographic Location, Weather	Between 0.1 and 0.3 Hz depending on conditions	Ranges from ±50 µGal-±350 µGal depending on weather, location and geology Earthquakes give very large but short disturbances.	Averaging over long measurement period, filtering of the raw data.
	Anthropogenic Noise (Vibrations)	Time, Location, Geology	Broadband range but generally higher frequency than microseism noise (> 0.5 Hz)	Highly dependent on activity	Avoiding trouble spots, taking longer duration measurements, filtering and despike routines on the raw data.
	Wind Noise	Time, Weather, Location	Higher frequencies (> 0.5 Hz) but often in short pulses due to gusts of wind	Dependent on weather and if the measurement location is exposed	Windshield (elimination), filtering and despike routines, averaging over a long measurement period (reduction)

Method and Processing

In order to separate these sources of noise, it is necessary to take measurements with multiple instruments simultaneously [23] to assess the long-term stability of the instrument and repeatability of the measurements. Measurements were taken using three Scintrex CG5 instruments simultaneously (hereby designated Scintrex A (serial number 40867), Scintrex B (serial number 40437) and Scintrex C (serial number 40018)) for 37.5 hours between 19th-21st June 2015. All three instruments had their temperature and tilt sensitivities recently calibrated using the procedures specified in the operating manual [1]. Data were acquired on a static point in the sub-basement of the Gisbert Kapp building in the University of Birmingham, UK (Figure 2). This location had the advantage of being shielded from wind and other sources of anthropogenic vibrational noise such as traffic allowing a detailed study of instrumental and microseism noise to be carried out and represented idealised conditions for a microgravity survey allowing the theoretical limitations of the instrument to be established. The clocks were synchronised using the GPS attachment supplied with the instrument, and left to warmup in-place for a 20 minute period to allow the instrument to stabilise after transportation as a result of elastic relaxation of the spring due to tilting and vibration effects [1, 5, 16]. The three instruments were then started simultaneously using a single remote control to run continuously in 256 second cycles (the maximum allowed by the CG5's software in order to leave as few gaps in the data as possible). Raw data logging was also enabled in the instrument's software to acquire the 6 Hz sampled data from the analogue-to-digital converters within the instrument, which was necessary to examine noise sources with periods shorter than the measurement cycle time including microseism noise and vibrational noise from nearby man-made sources.

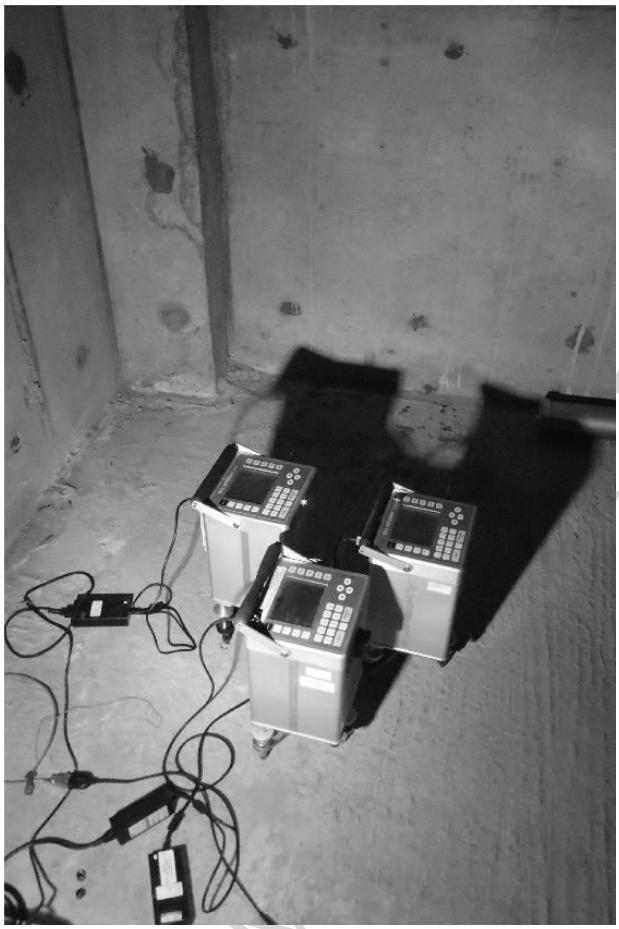

Figure 2: The three instruments used to characterise the noise in the basement in the University of Birmingham

The effects of different processing techniques on the data are shown in Figure 3. Data from each of the instruments were corrected individually for temperature and tilt using data from the internal sensors and equations given in the Scintrex's operating manual [1] and the relevant parameters from the individual instruments. An example of this processing is shown in Figure 3. Measurements were first corrected for temperature variations using the inbuilt temperature sensors and the temperature correction coefficient and offset acquired from Scintrex (Figure 3b). A mistake was found in the formula in the manual for converting the ADC counts to tilts in arcseconds and the correct version was used and confirmed with Scintrex (Equation 1).

$$X_{obs} = \left(\left((ADC_X \ \ 0.000076295 - 2.5\ )Sensitivity_X\right) - Offset_X\right) \quad [1a]$$

$$Y_{obs} = \left(\left((ADC_Y \ \ 0.000076295 - 2.5\ )Sensitivity_Y\right) - Offset_Y\right) \quad [1b]$$

Where *ADC* is the value from the analogue-to-digital converter recorded in the file and *Sensitivity* and *Offset* are the tilt sensitivity and tilt offset values stored in the instrument's firmware during calibration respectively (Figure 3c). Further details on processing raw data from the Scintrex CG5 to remove instrumental effects are provided by Sugihara [22]. Celestial tides were removed using an ephemeris model [24] (Figure 3d) and the residual ocean tide corrected using an ocean tidal loading model [25] (Figure 3e). Finally, instrumental drift, caused by relaxation of the instrument's quartz spring (described as approximating a linear process over the typical duration of a survey) needed to be removed (Figure 3f). In typical surveys, this is implemented by taking repeat measurements on a single base station point throughout the survey day to assess the observed changes in gravity measurements after other corrections for time-varying effects have been applied. However, since the measurements were taken in a static location with non-varying gravity, the whole dataset was drift corrected by removing a linear trend. As the instrument positions were fixed, no further data reduction techniques due to the locations of the instruments (e.g. latitude, free air and Bouguer corrections) were necessary. Preliminary examination of the data by averaging the individual measurement cycles showed that even with the corrections, a residual tidal effect (with a period of roughly 12 hours) existed which was visible on all three instruments (Figure 4). In practice, it is possible to remove this unwanted signal with good survey practice and the removal of a higher-order polynomial fit for the removal of drift, if base station measurements or repeated points are taken with sufficient frequency (at least once per hour). For this reason only sources of noise above the frequency of this tidal signal (> $1x10^{-5}$ Hz) were of concern and the remaining tide was removed using a 6^{th} order polynomial fit, or equivalent band-pass filtering.

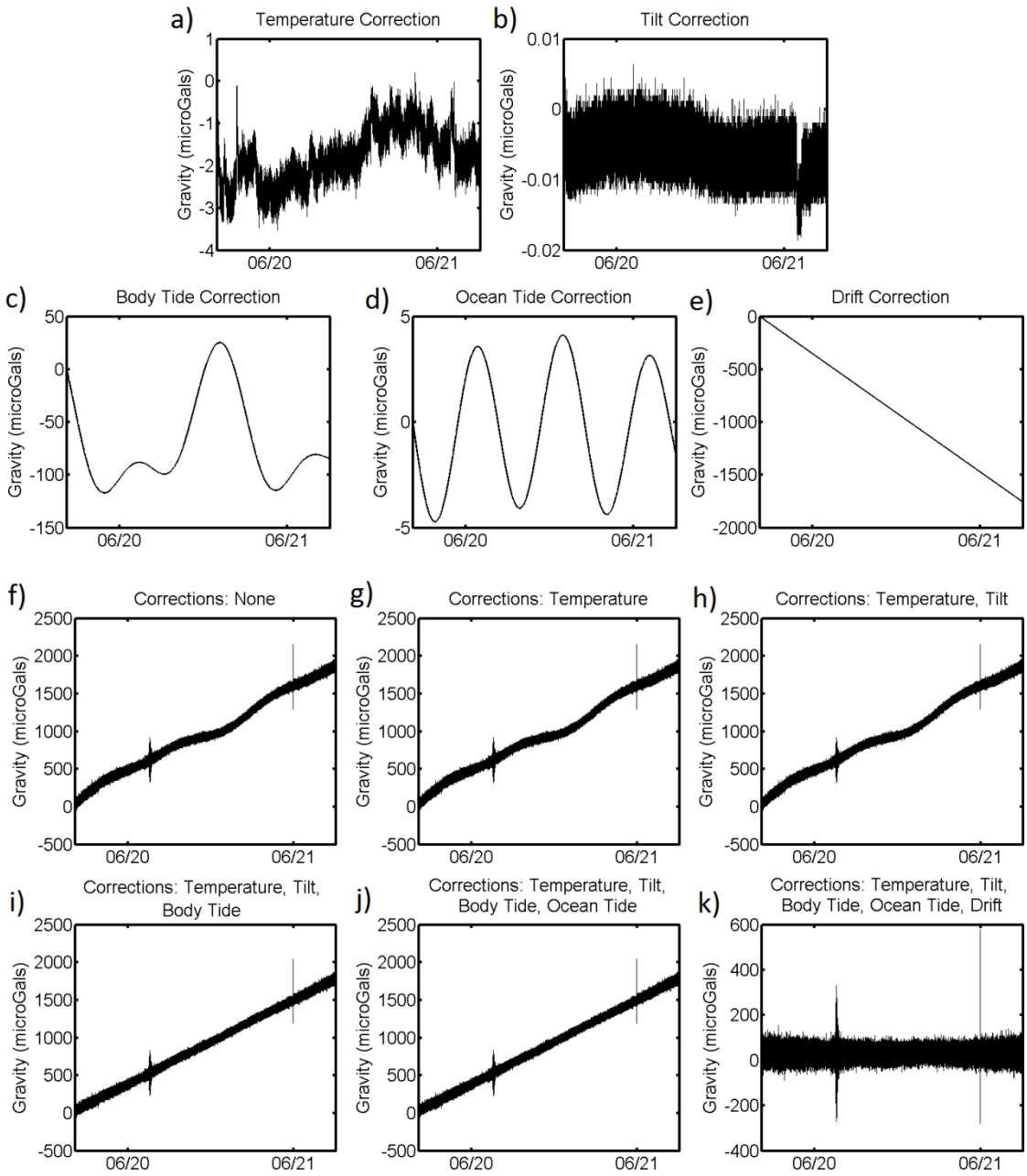

Figure 3: Examples of the different corrections applied to the gravity data a) temperature correction b) tilt correction c) Celestial tidal correction d) ocean tidal loading correction and e) drift correction. The effects of these different corrections on raw gravity data are also shown f) No corrections g) Temperature corrected h) Temperature and tilt corrected i) Temperature, tilt corrections and celestial tidal model applied j) Temperature, tilt corrections and celestial and ocean tidal models applied k) Temperature, tilt corrections and celestial and ocean tidal models applied then corrected for drift using linear trend.

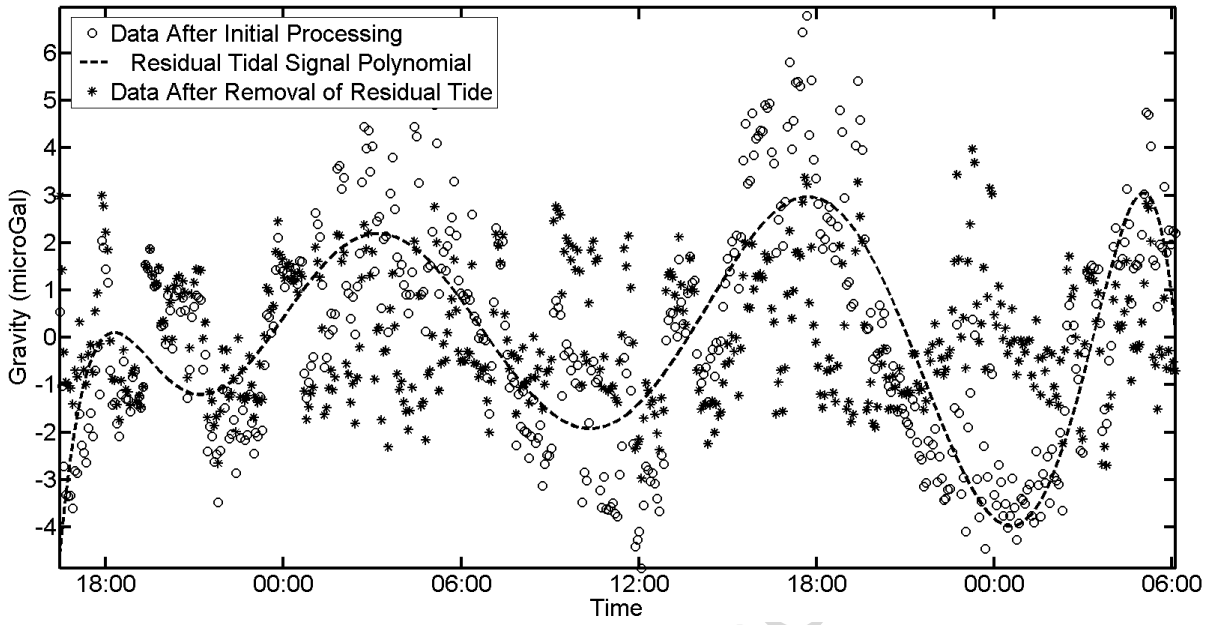

Figure 4: The residual tidal signal after data processing steps shown in figure 3 and removal with a polynomial fit

Results and Analysis

In order to better understand the nature of the different noise signals and the frequencies at which they operate, a fast Fourier transform (FFT) was applied to the corrected 6 Hz data for the three instruments (Figure 5) used to measure in the University of Birmingham basement. "Real" environmental sources of noise should be visible on all three instruments whereas the instrumental noise due to differences in the sensors and electronics between instruments should vary. In the absence of wind and industrial vibrations, the main source of environmental noise originates from seismic vibrations such as those caused by the ocean waves [19]. This noise is visible as two main peaks which are at similar frequencies on the data from all three instruments; the main microseism noise showing as a peak between 0.2 and 0.3 Hz and a lower frequency seismic at around 0.1 Hz which occurred during a magnitude 6.4 earthquake in Chile [26]. The spectral resolution limits of typically encountered integration periods are included to show that microseism spectral features will be included within the associated signal processing operations.

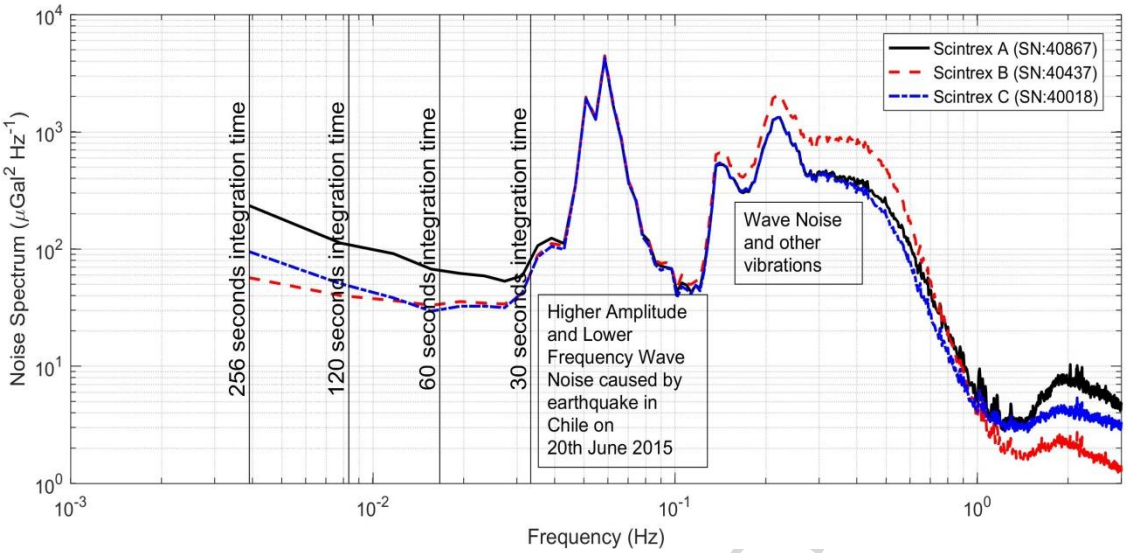

Figure 5: FFT analysis of 37.5 hours of data collected using 3 Scintrex CG5 instruments simultaneously. Peaks at similar frequencies are shown within the measurement cycle but the instrument noise predominantly affects the lower frequencies

In contrast the noise sources which differ between the instruments fall at much lower frequencies, below the minimum spectral resolution of the instrument corresponding to the reciprocal of 256 seconds, meaning these cannot be effectively averaged out within the measurement cycle. These sources of noise represent the practical limitation of the instrument even in a low-noise environment. According to the Scintrex manual [1], the error on an individual measurement can be expressed using equation 2 which makes the assumption that the noise during the measurement cycle is white.

$$error = \frac{SD}{\sqrt{DUR}} \qquad [2]$$

Where SD is the standard deviation and DUR is the measurement duration in seconds. The spectra presented in Figure 5 clearly illustrates that the noise cannot be assumed to be white and more appropriate signal processing formulations will be presented in the next section.

Calculation of the standard deviation values for the three instruments (Figure 6a) showed that the error on all of the measurements over the monitoring period was below the resolution of the instrument (1 µGal), with the exception of the period during the earthquake, where background

microseism noise was higher than usual. However, because the frequencies of the instrumental source of noise fall below the reciprocal of the integration times of the measurements, this method underestimates the true errors (Figure 6b). Taking the mean value of the whole period (507 measurments) as the "true" value of gravity, the same data can be used to show the deviation from this value for each instrument as a probability density function to assess the frequency of occurrence of instrumental errors in Figure 7. This shows that the practical limitation on the accuracy of a given measurement is limited by the instrumental noise and the limitation of the measurement cycle to 256 seconds.

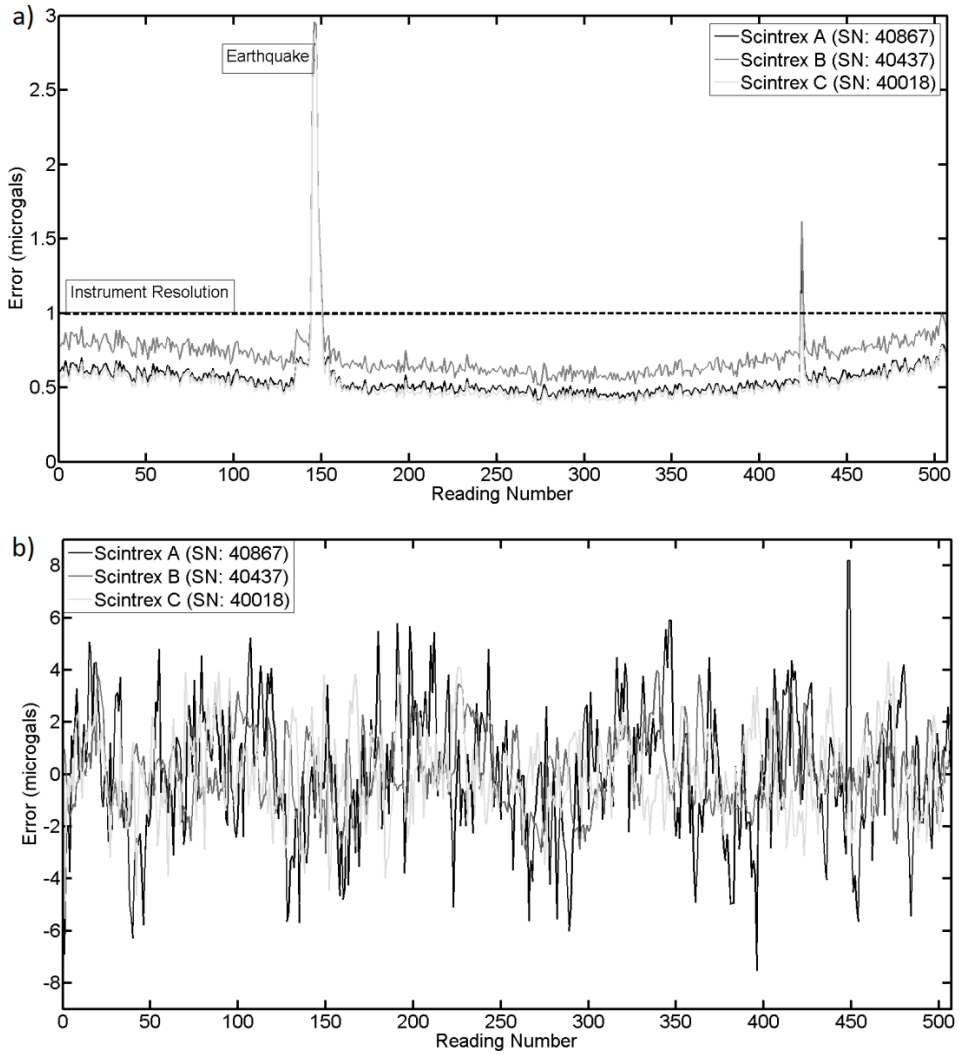

Figure 6: a) The error of the mean on individual 256 second measurements representing the efficacy of the averaging process on removing environmental noise and b) the actual errors of the measurements from the three instruments

From this it can be concluded that errors, consequent accuracy and repeatability of gravity measurements using existing equipment are determined by two main factors:

1. The ability to integrate individual measurements for long enough to remove environmental signals or reduce their effects through signal processing filters such as those discussed later. This can be estimated using the standard deviation of the measurement and measurement duration and should be the focus of further noise reduction to both increase measurement speed and accuracy.
2. Instrumental noise with a period longer than the maximum measurement time, which in practical terms manifests as a pseudo-normally distributed noise with standard deviations between 1.43 and 2.49 µGal (typically giving a maximum noise of between ±4-8 µGal) depending on the instrument. This source of noise can only be removed by using repeated measurements on each spatial point which reduce the error by an amount proportional to the square root of the number of measurements.

The optimum measurement time should be long enough to integrate the higher frequency noise while being sufficiently short to avoid being influenced by lower frequency sources of noise containing incomplete cycles which manifest as drift. This can be assessed using the Allan deviation (Figure 8) which assesses the stability of measurements for different measurement cycle lengths. At shorter measurement times for all three instruments the deviation decreases as the noise processes average out whereas at longer times, the deviation increases due to the drift from instrument noise. The optimum measurement time can be found at the minimum values of deviation which for all instruments is 120-200 seconds.

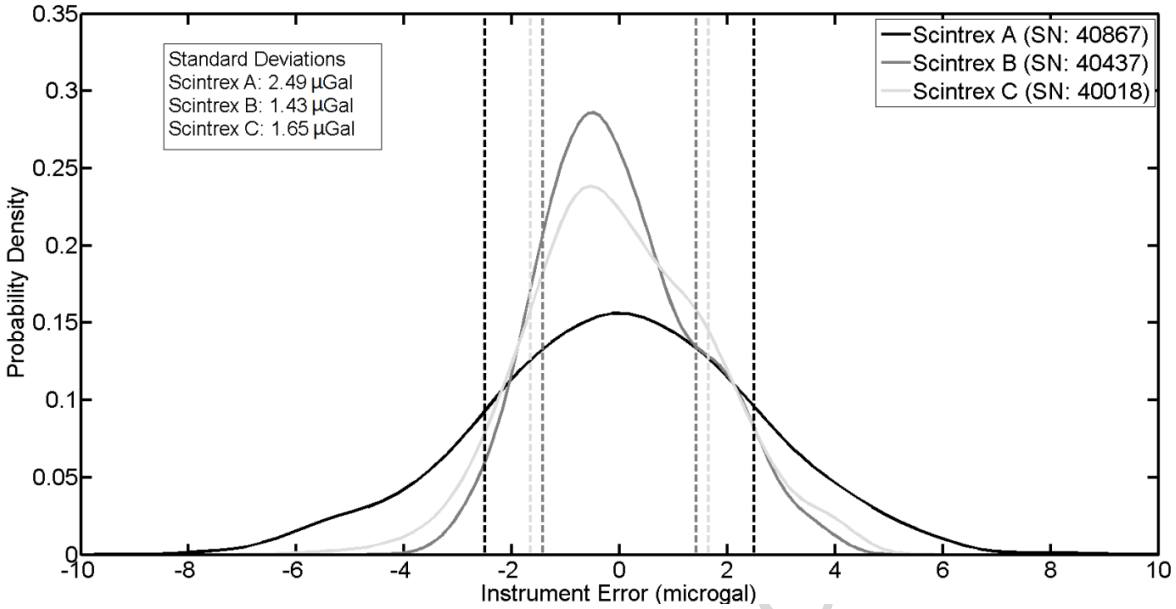

Figure 7: Probability density function of instrumental errors expressed as deviation from the mean value after all environmental signals have been removed

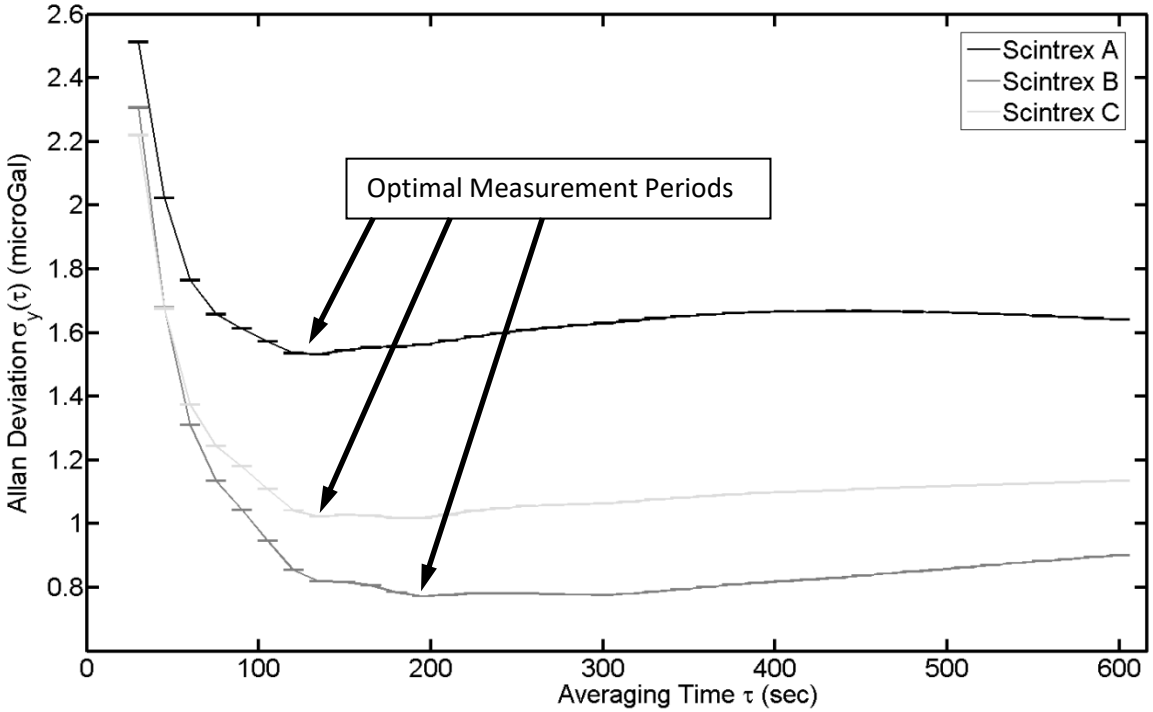

Figure 8: The overlapping Allan Deviation of the long period measurements

Survey Quality Improvement Techniques by Reduction of Environmental Noise

Gravity surveys are often conducted in urban areas, near busy roads or at construction sites which contain sources of high-frequency industrial and anthropogenic vibration noise. Gravity measurements in the countryside or in open areas may be also affected by wind. The air turbulence is a source of additional high-frequency vibrations. Pressure differences between the upwind and downwind sides of the measuring device can tilt the instrument, adding an additional low-frequency error to the measurements.

The simplest way of improving data quality is to increase the duration of measurements. In this case, the error of the data decreases by a factor proportional to the square root of the measurement's duration [27]. The typical gravity survey for shallow targets has a measurement spacing of 2-8 m [e.g. 12] and can cover areas of a few hundred to several thousand square metres depending on the targets and area of interest and thereby contains hundreds of points. Increasing the duration associated with each measurement therefore leads to a significant increase in the overall duration of the survey and makes use of the instrument less efficient. Thus any technique that can reduce the total survey duration is worthy of consideration.

The task of the surveyor and data analyst is to estimate the gravity signal, $y(t)$, using a process illustrated in Figure 9. The actual gravity signal is denoted by, $s(t)$, and is assumed to be a constant in a time-invariant landscape. However, this signal is contaminated by a multitude of additive environmental noise source discussed earlier with a power spectral density $G(f)$. The estimate is calculated using a matched filter, implemented by convolving the measured time-domain signal with a linear time-invariant filter impulse response, $h(t)$. The coefficients, $h(t)$, are chosen such that the signal-to-noise ratio of the estimate, $y(t)$, is maximised.

A conventional average (boxcar) is optimal when the noise spectral density is white. Thus given a data collection record window (measurement cycle time) of duration, τ , and a white noise spectral density.

$$h(t) = \frac{1}{\tau} \text{ for } 0 \leq t \leq \tau \quad [3a]$$

$$h(t) = \ 0 \text{ elsewhere} \quad [3b]$$

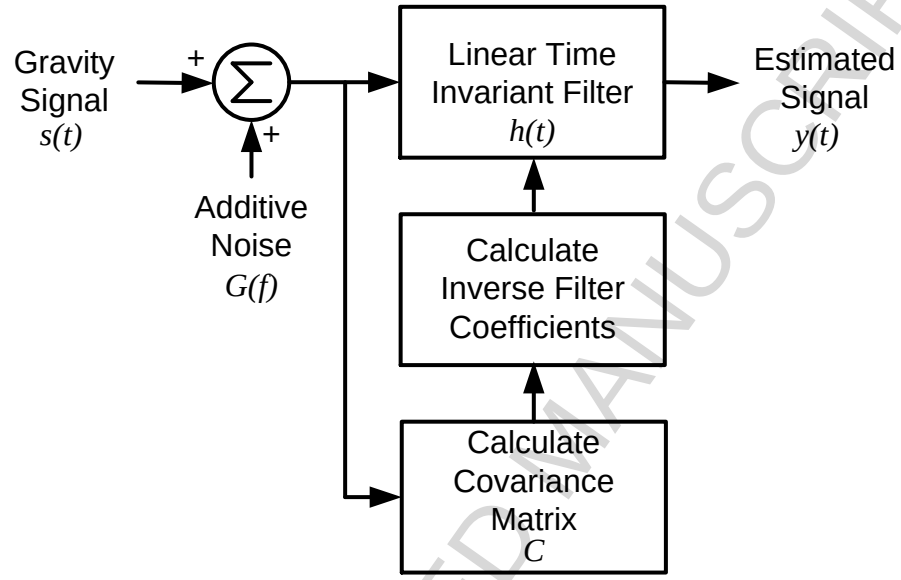

Figure 9: Mean estimation using linear time-invariant filter

However, as shown in the results above, the microseism noise is not white, but has a characteristic peak frequency between 0.1 and 0.3 Hz. When the noise can no longer be assumed to be white, as in all the results presented within this paper, the power spectrum must be estimated from the sensed data. One approach is to calculate the sampled covariance matrix, $\mathbf{C}$ [27]. This is a symmetric square matrix of dimensions *N* by *N*, typically where *N* is the number of data values collected per record at each spatial survey position (*N*=180 for a 30 second measurement cycle time as used by many commercial Scintrex CG5 surveys). For example, for a matrix representing a large number of measurement records, $\mathbf{s}$, each consisting of three samples, the covariance matrix would be

$$\mathbf{C}=\begin{bmatrix} E\left[(s_1-\mu_1)(s_1-\mu_1)\right] & E\left[(s_1-\mu_1)(s_2-\mu_2)\right] & E\left[(s_1-\mu_1)(s_3-\mu_3)\right] \\ E\left[(s_2-\mu_2)(s_1-\mu_1)\right] & E\left[(s_2-\mu_2)(s_2-\mu_2)\right] & E\left[(s_2-\mu_2)(s_3-\mu_3)\right] \\ E\left[(s_3-\mu_3)(s_1-\mu_1)\right] & E\left[(s_3-\mu_3)(s_2-\mu_2)\right] & E\left[(s_3-\mu_3)(s_3-\mu_3)\right] \end{bmatrix} \quad [4]$$

Where *E* is the expectation and the mean $\mu = E[\mathbf{s}]$. To ensure that the covariance matrix is non-singular, the total number of sampled gravity measurements must exceed N^2. This requirement would normally be achieved within a single day during commercial survey operations. Should fewer data samples be available, then the size of the covariance matrix would be reduced, typically by digitally low-pass filtering the input data records and re-sampling at a lower rate, or by sub-dividing the data records into snapshots of shorter duration.

Having obtained the covariance matrix, the best linear unbiased estimator (BLUE) [28] may be calculated by

$$\mathbf{y}=\left[\mathbf{1}^T\mathbf{C}^{-1}\mathbf{1}\right]^{-1}\mathbf{1}^T\mathbf{C}^{-1}\mathbf{s} \quad [5]$$

Where $\mathbf{1}$ is an *N* by 1 column matrix populated with ones, $\mathbf{1}^T$ is the transpose of $\mathbf{1}$ and $\mathbf{C}^{-1}$ is the inverse of the covariance matrix $\mathbf{C}$. This process may be considered as that of calculating a pre-whitening filter with coefficients

$$\mathbf{h}=\left[\mathbf{1}^T\mathbf{C}^{-1}\mathbf{1}\right]^{-1}\mathbf{1}^T\mathbf{C}^{-1} \quad [6]$$

Thus, if a typical 30 second data collection record contains 180 samples, the linear time-invariant filter illustrated in Figure 9 will also comprise of 180 samples and a single sample will be computed for the signal estimate $y(0)$.

Background Microseismic Measurements

To demonstrate the efficacy of this data-driven filtering approach, the data collected from the three Scintrex CG5 instruments located in a basement of the University of Birmingham was analysed.

These instruments were set to collect data for 37 hours, equating to 507 records of 1536 samples (256 second observation periods). The raw data from one Scintrex CG5 is shown in Figure 10. This shows regular microseismic activity and two transient events. The first is a magnitude 6.4 earthquake in Chile [26], the second is presumed to be an unknown local seismic event occurring in the middle of the night.

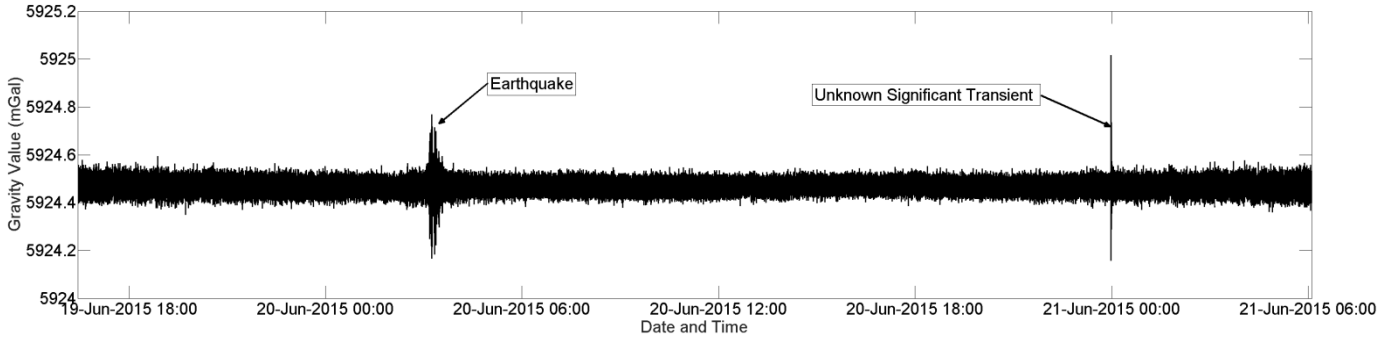

Figure 10: Raw data collected in sub-basement of building

In order to compute an invertible covariance matrix, $\mathbf{C}$, the data matrix, $\mathbf{s}$, was reshaped to a size of 768 by 1014 – corresponding to shorter, 128 second duration records. Any columns in the data matrix, $\mathbf{s}$, with a variance exceeding twice the mean variance for all remaining records were discarded. For the results illustrated in Figure 10, this process resulted in discarding fourteen columns of data.

A standard problem with any inverse filter approach will be that nulls in the input frequency spectrum will lead to very high peaks in the frequency response of the inverse filter. The commonly applied solution is to deviate from the optimum filter (BLUE) by equivalently adding uncorrelated noise to the input signal. In this case the peak frequency response of the filter was arbitrarily limited to +10 dB within the regions outside the nominal passband of the instrument, whilst ensuring that the ratio between the magnitudes of the largest to the smallest eigenvectors was less than 10^8 to ensure numerical resolution limitations did not affect the inversion of the covariance matrix.

The results of the data-driven frequency response of the filter are illustrated in Figure 11. The solid trace represents the inverse filter approach whilst the dashed line represents a conventional (boxcar) filtering approach. It will be noticed that the inverse filter effectively places nulls in the spectrum corresponding to maxima in the microseismic and instrument noise spectrum. The gain of the filter is correspondingly allowed to increase in regions of very little input spectral energy, such as approaching the Nyquist frequency (3 Hz). An improvement in estimator quality would be expected to correspond to regions where the filter response is supressed below that of the conventional (boxcar) response.

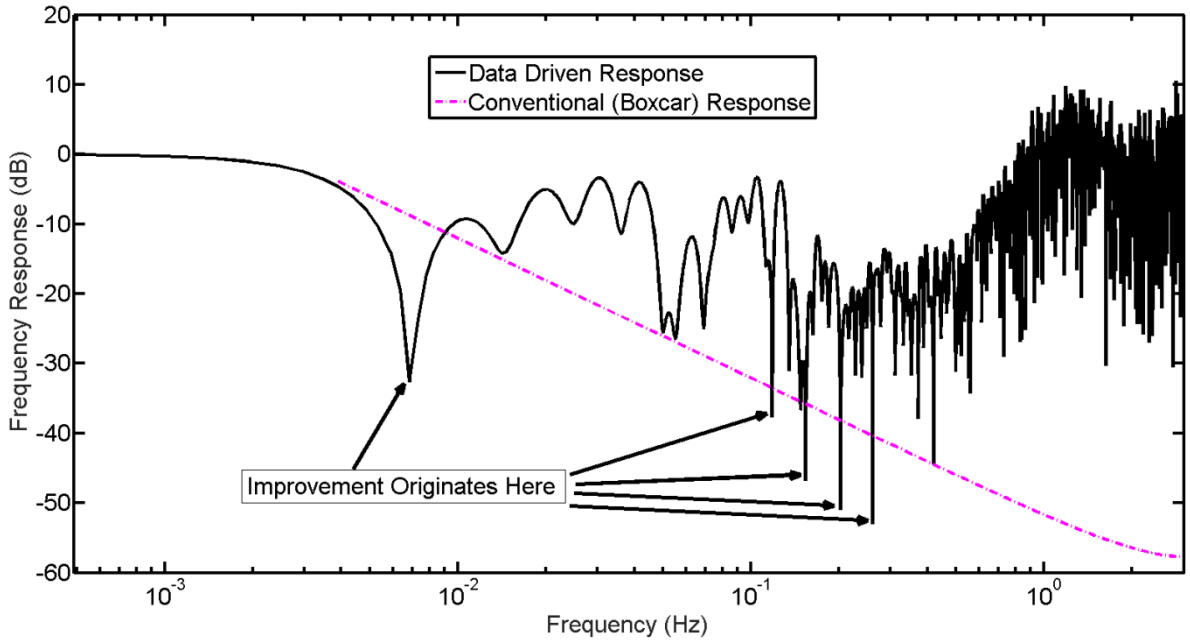

Figure 11: Data-driven filter response for an inverse filter approach with only microseismic and instrument noise present

To demonstrate the possible improvements of this approach for this measurement environment, the probability density functions of the estimators are plotted in Figure 12. The mean of the inverse filter distribution has been subtracted from the other distributions for visual clarity, random mean value offsets of the various estimators will remain. All other low-frequency (<0.001 Hz) periodic residuals were removed by filtering before computing the statistical distributions. The solid trace corresponds to the inverse filter (BLUE) and yields a standard deviation of 1.48 µGal, the dotted line

represents the internal Scintrex seismic filter algorithm and yields a standard deviation of 2.15 µGal, whilst the dashed line represents a conventional (boxcar) averaging process and yields a standard deviation of 2.48 µGal. The summary is that under these measurement conditions, the use of a more sophisticated filtering approach would result in a 40% reduction in measurement uncertainty, or the same uncertainty being obtained in 35% of the original measurement time.

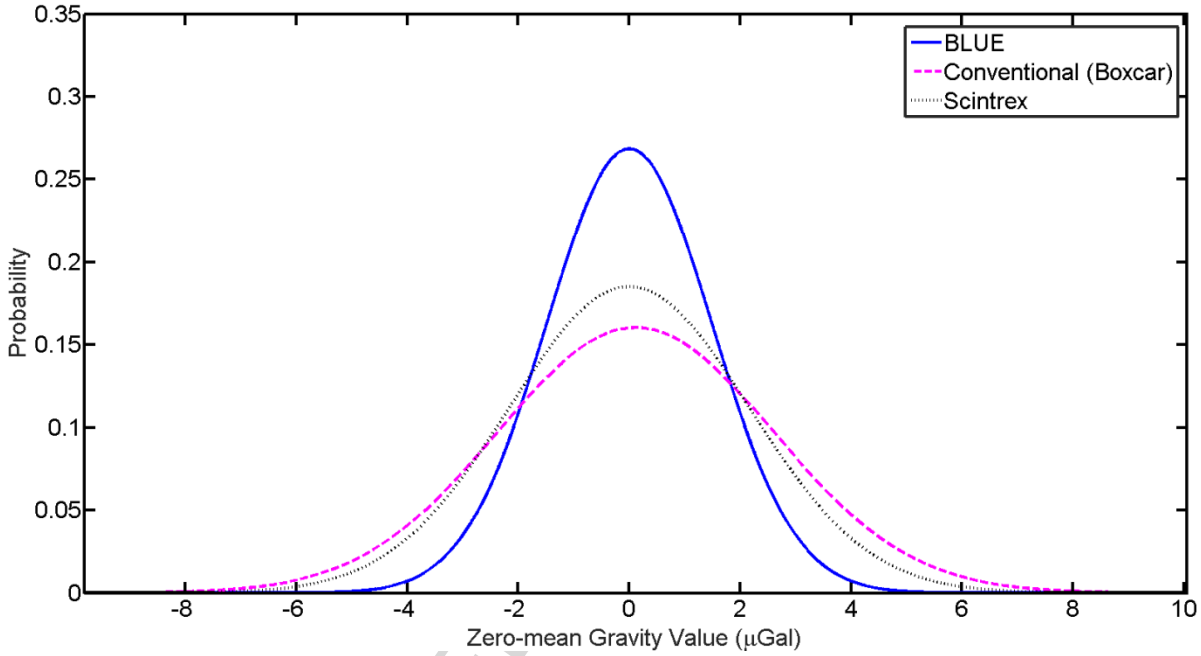

Figure 12: Probability density function of three different estimators with only microseismic and instrument noise present

Traffic Noise and Transient Removal

Conventional gravity surveying wisdom states claims that local traffic noise and related impulses degrades survey quality. To test this hypothesis, a Scintrex CG5 was located in a gas bottle storage room about 5 m away from an urban road with a moderate traffic density comprising cars and laden commercial vehicles. The foundations of this small room were of comparable depth to the road foundations and the instrument would have been well-shielded from short-term air pressure variations. It is believed that this scenario represents the closest a real gravity survey could get to an active roadway. Data were collected over a period in excess of 8 hours and the raw data are

presented in Figure 13. This data set reveals a surprising result in that very few transients are identifiable manually and that the magnitudes of these events are relatively small.

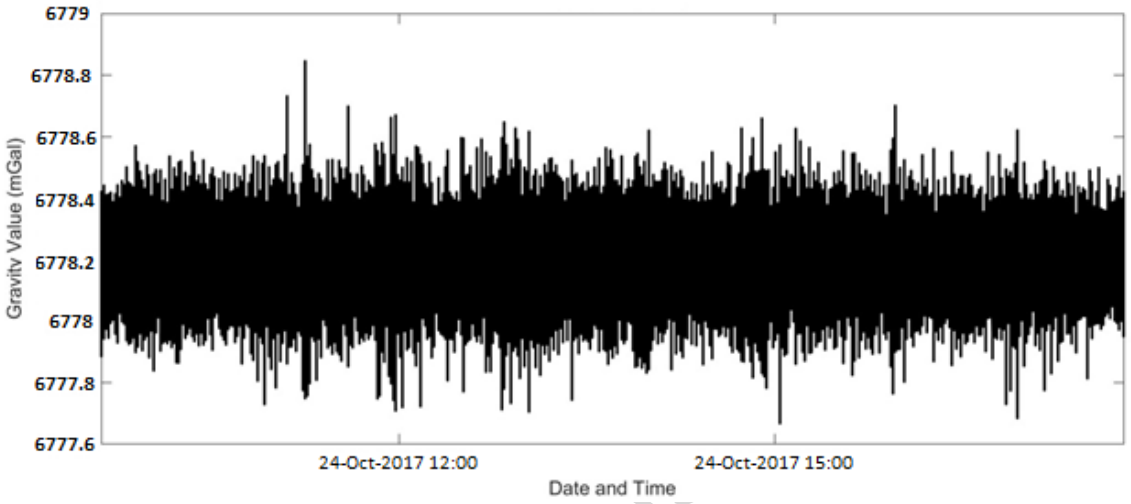

Figure 13: Raw data collected next to road with moderate traffic density

Of the 453, 60-second data records, two were rejected as their variance exceeded twice that of the mean for all remaining records. The frequency response of the inverse filter calculated from this data is shown in Figure 14. Remarkably, the characteristics of the inverse filter are very similar to those of Figure 11, even though the originating data was significantly contaminated by traffic noise.

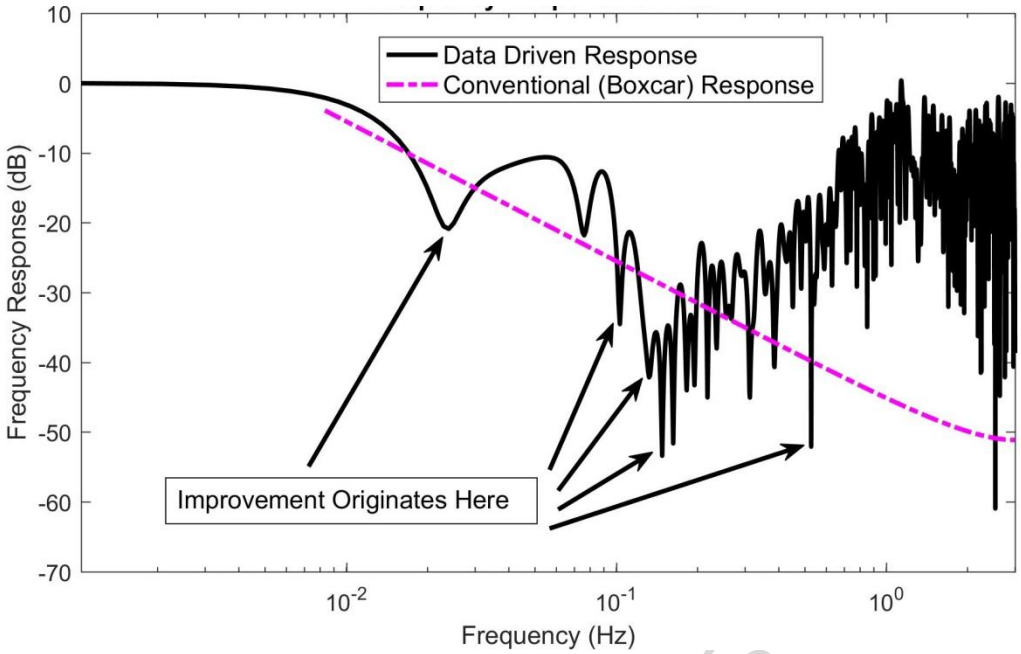

Figure 14: Data-driven filter response for an inverse filter approach with microseismic, instrument noise and significant traffic noise present

The probability density functions of the estimators are plotted in Figure 15. The solid trace corresponds to the inverse filter (BLUE) and yields a standard deviation of 1.87 µGal, the dotted line represents the internal Scintrex noise reduction processes and yields a standard deviation of 3.47 µGal, whilst the dashed line represents a conventional (boxcar) averaging process and yields a standard deviation of 3.81 µGal. The summary is that in the presence of significant traffic noise, the measurement uncertainty has typically increased by between 25% and 50% - a surprisingly small increase. Thus, it is possible that the anecdotal evidence of traffic noise reducing the quality of gravity surveys is due to the air pressure waves from the vehicles affecting the alignment of the instrument, rather than originating from a ground-coupled effect.

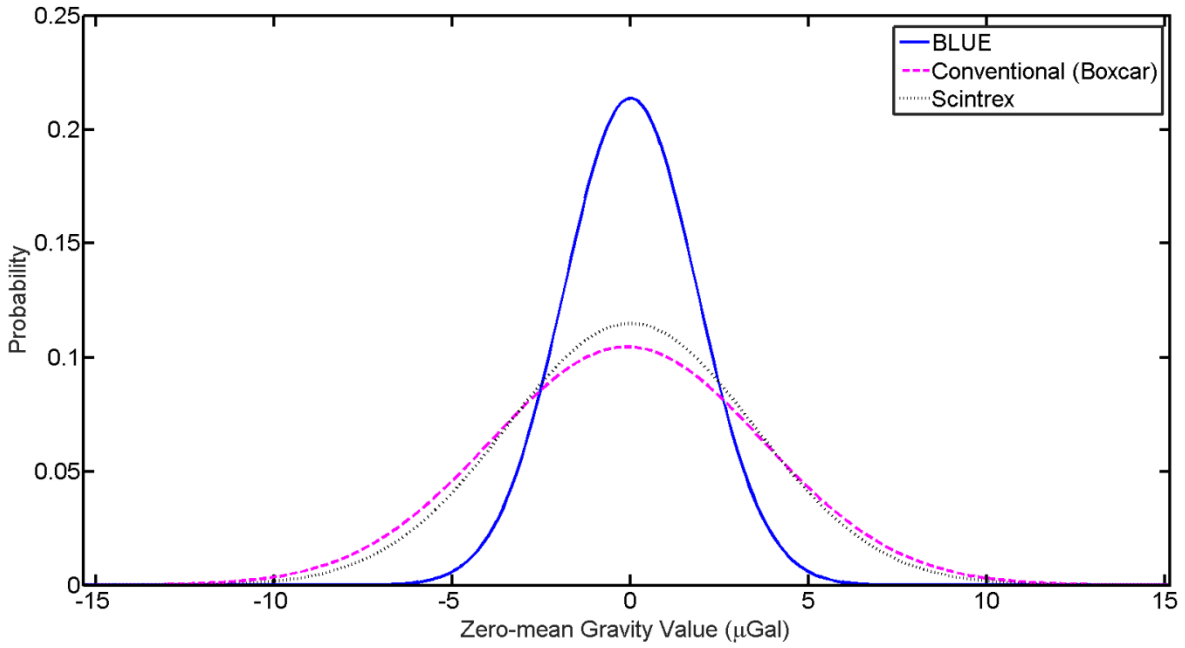

Figure 15: Probability density function of three different estimators with microseismic, instrument noise and significant traffic noise present

Current surveying practice usually rejects complete records, based on the variance of the data exceeding some pre-defined constant. The discarding of individual transients whist still processing the remainder of the data record is of interest to the gravity surveyor. To detect transients the algorithm proposed by Hassanpour, et al. [29] was used. Spectrograms of the gravity signal in the time-frequency domain were calculated using short time Fourier transforms with a 32-sample and a 75% overlapping window computed in Matlab. The results were analysed at frequencies of 1.7 Hz, 1.9 Hz and 2.1 Hz. A constant probability of false alarm (CFAR) detector was implemented with a detection threshold of +17 dB corresponding to probability of false alarm of 10^{-14} under normally distributed white noise conditions. Samples were classified as a transient if two, or more, of the three analysis bands triggered their respective CFAR detectors. An example of an automatically detected transient event is illustrated in Figure 16. The top trace shows a typical 60-second raw data record with the characteristic signature of a heavy vehicle passing the sensor – the detected samples are highlighted with circles. The second trace shows the spectrogram, with vehicle noise being characterised by spectral components with frequency content in excess of 2 Hz. The third trace shows the energy content in the three, higher-frequency analysis bands – indicating that transient

events manifest across multiple bands. The fourth trace illustrates a constructed cosine-tapered window used to reduce the effects of transient events on the estimation process. This is generated by equation 7.

$$w(n) = 0 \quad \text{for} \quad 0 \le |n| \le \frac{k}{2}$$

$$w(n) = 1 - 0.5\left[1.0 + \cos\left(\frac{\pi\left(n - \frac{k}{2}\right)}{(N-k)}\right)\right] \quad \text{for} \quad \frac{k}{2} \le |n| \le \frac{N}{2}$$

$$w(n) = 1 \quad \text{for} \quad |n| \ge \frac{N}{2} \qquad [7]$$

where *N* represents the number of samples equivalent to the duration of the transient and *k* represents the number of samples in the slopes of the window function.

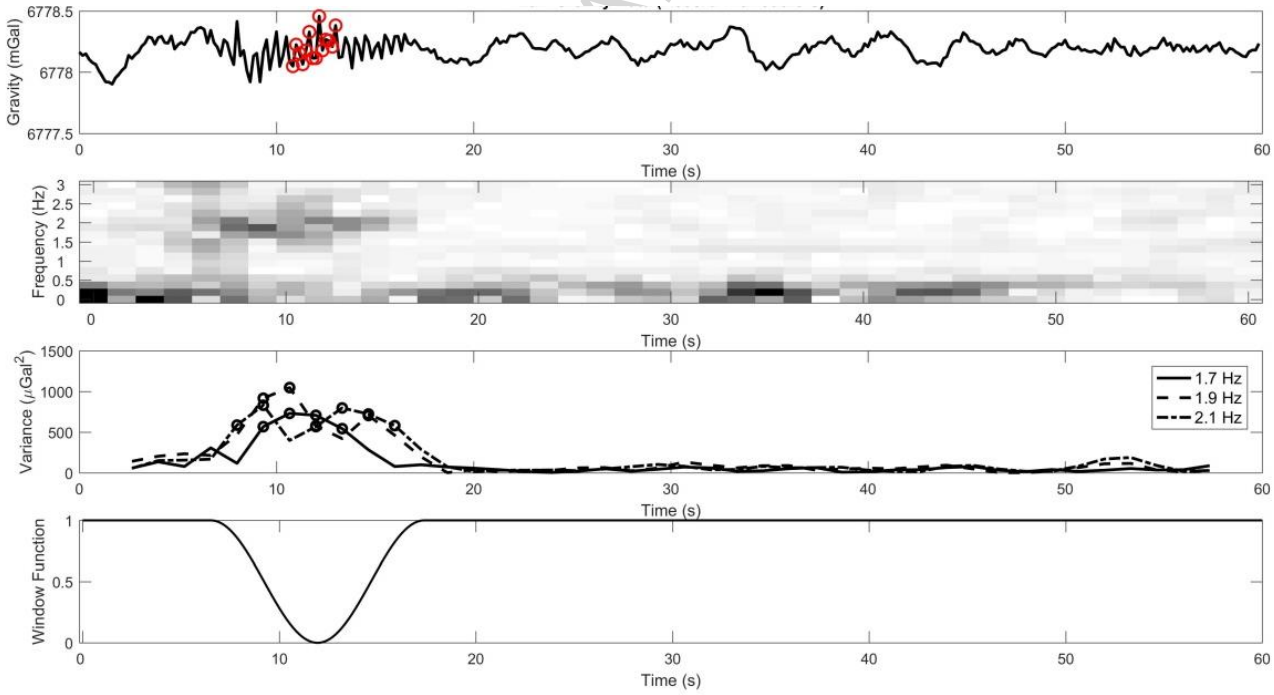

Figure 16: One example of an automatically detected traffic noise event

Implementing an automatic traffic event suppression filter on the 451 data records yielded 1.7% of data samples were contaminated by traffic noise. Applying a constructed cosine-tapered window to reject such events prior to a conventional (boxcar) averaging process made no discernible difference

to the statistics of the estimation process. However, the data-driven filtering approach was significantly degraded as the cosine-tapered window adds spectral content to frequency domain regions amplified by the inverse filter. In summary, ground-coupled traffic noise appears to be partially coherent in nature and is well supressed by either a data-driven inverse filter approach, or a conventional (boxcar) filtering approach. The use of selective event-suppression windowing does not appear to be effective.

Wind Noise Reduction

It is well-known that wind has a significant effect on the quality of a gravity survey and wind deflectors are routinely deployed. To isolate the typical impact of wind noise, data were recorded using Scintrex CG5 for 13.3 hours on 28th Oct 2017. A location was chosen remote from any traffic noise and subject to turbulent wind vortexes. Automatic detection of transient events was again employed, and a typical transient is illustrated in Figure 17. The detected event is identified with circles superimposed on the data points; all similar wind-induced transients are very much shorter than the traffic-induced events and have spectral content at higher frequencies.

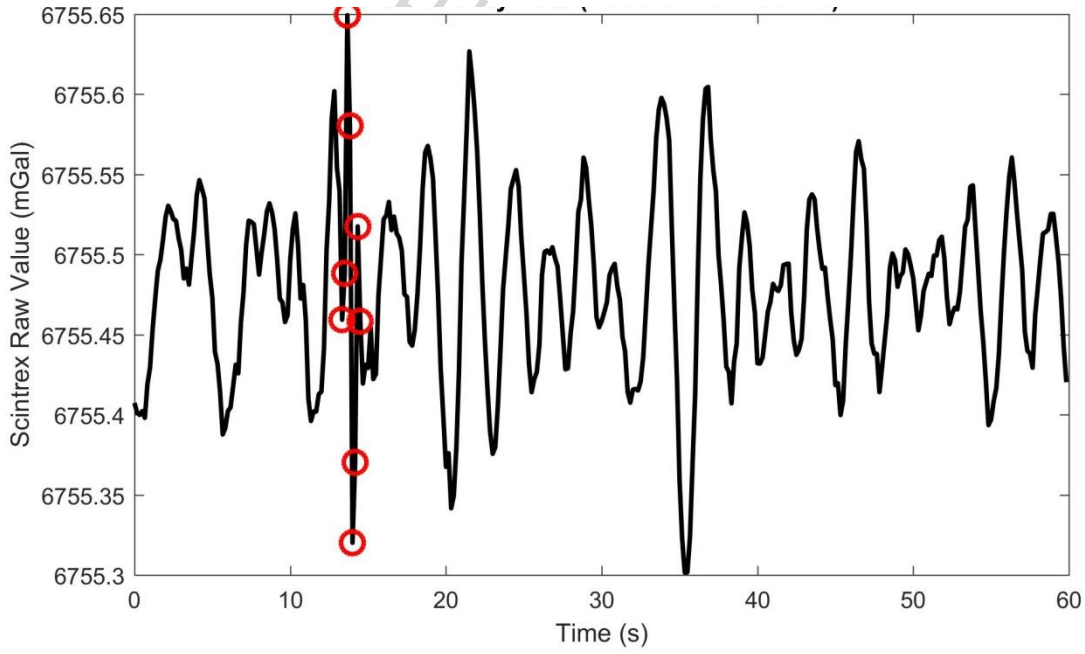

Figure 17: One example of an automatically detected wind-noise event

The probability density function of the estimators was again computed. The inverse filter (BLUE) yields a standard deviation of 1.60 µGal, the internal Scintrex seismic filter process yields a standard deviation of 2.78 µGal, whilst the conventional (boxcar) averaging process yields a standard deviation of 2.71 µGal. This data set reveals that the inverse filter cannot be time-invariant. The standard deviations quoted were for a covariance matrix estimated using 6 hours of data. When the covariance matrix was computed using the full 13.3 hours, the inverse filter performed slightly worse than the conventional (boxcar) filtering process. The spectral characteristics of the microseismic activity were observed to slowly evolve during this period.

Commercial Survey Results

The data presented thus far show that a data-driven inverse filter approach can provide useful gains, even in the presence of traffic and wind noise. The statistical analysis of a real gravity survey is more challenging as the value of the desired estimator in unknown and spatially varying.

It was initially assumed that all measurement records could be utilised to compute the covariance matrix and hence the inverse filter. Interestingly, this led to a set of filter coefficients approximating a raised cosine window (a modified Hann window) with performance very similar to that of the conventional (boxcar) window. Further investigation revealed that a multiplicative noise source was responsible for this, or that the instrument gain associated with the microseismic activity varied from survey position-to-position. Two reasons are postulated for this effect; that the ground compliance provides a locally varying attenuation of microseismic activity, or that the tilt sensor correction introduces a tilt-related attenuation.

However, common practice is to correct for instrument drift by returning to a fixed station position at regular intervals. The gravity value is assumed to be constant at this location and may thus be used to present meaningful statistical measures and provide data for the computation of the covariance matrix. As a typical example, the 31st Oct 2017 was randomly selected as a single day of a commercial gravity survey being conducted at Broadway, Worcestershire, UK. The surveyors

collected 265, 30-second records in a day, of which 42 interspersed records were collected on a fixed station point. To compute an invertible covariance matrix, these 42 records were sub-divided into 126, 10-second records of which six were discarded because their variance exceed twice that of the mean variance of the remaining records. Thus, with a 6 Hz sampling rate, a 60-point inverse filter was computed for this day. The inverse filter (BLUE) yields a standard deviation of 3.73 µGal, the internal Scintrex seismic filter yields a standard deviation of 5.99 µGal, whilst the conventional (boxcar) averaging process yields a standard deviation of 7.93 µGal. In summary, the data-driven inverse filter approach appears to be able to provide a worthwhile improvement in estimator quality in a field environment where the instrument is being repeatedly returned to a fixed station position.

Table 2 summarises the standard deviations of multiple measurements collected at fixed station points and at different times. Both traffic noise and wind noise lead to increased standard deviations. The greatest effect appears to be from manually handling the instrument by repeatedly moving the instrument to-and-from the station position. In all situations, a significant improvement appears possible by using a filter optimised for the non-white noise spectrum conditions prevalent at the time of the survey.

Table 2: Comparison of fixed survey position standard deviations under varying environmental conditions for realistic observation times

	Microseismic activity only standard deviation	**Microseismic activity + traffic noise standard deviation**	**Microseismic activity + wind noise standard deviation**	**Commercial field survey standard deviation**
Data-driven, inverse-filter approach	1.48 µGal	1.87 µGal	1.60 µGal	3.73 µGal
Internal Scintrex algorithm	2.15 µGal	3.47 µGal	2.78 µGal	5.99 µGal
Conventional (boxcar) filter	2.48 µGal	3.81 µGal	2.71 µGal	7.93 µGal

Further Testing in Field Conditions

In order to further test the data-driven inverse filter in field conditions, an anomaly of a known size was needed to assess the effects of filtering on the truth-data signal. An experiment was conducted in a car park, near to the University of Birmingham, UK. A line of data was collected using a scaffold tower over the middle of two stacks of concrete blocks, which were supplied with a known size and weight, allowing the density contrast to be accurately calculated (Figure 18a). The measurement points and the blocks were accurately located using a total station (Leica TS15) and the position of both is also shown in Figure 18b.

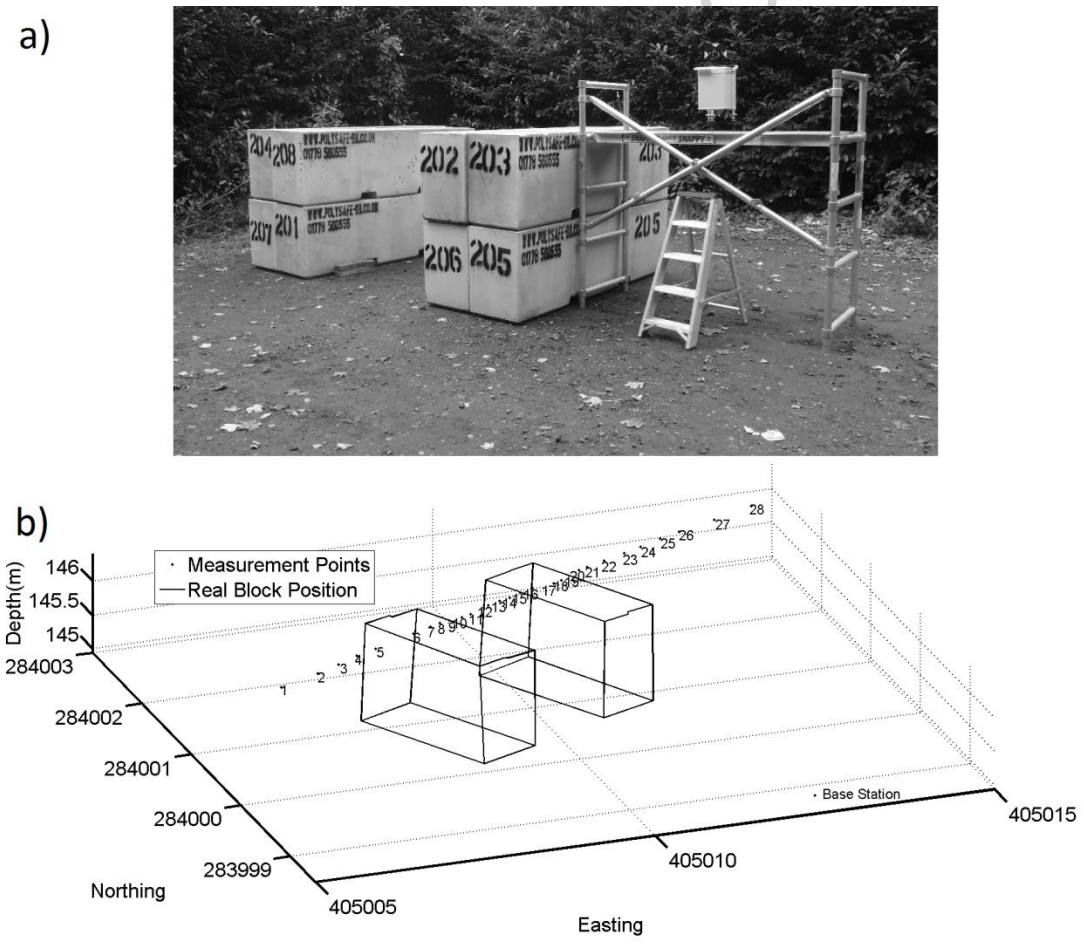

Figure 18: a) The experimental setup for field testing and b) the locations of the measurement points and concrete blocks

The instrument was set to collect raw 6 Hz data, which were corrected for instrumental errors (temperature and tilt) and celestial and ocean tides using the same methods as in the previous

experiments and drift was removed using repeated measurements throughout the day taken on a fixed base station. Several different filtering techniques were used on this data to create a number of comparative datasets:

1. Data were left unfiltered and averaged over the measurement cycle in order to assess the effects of a conventional (boxcar) filter (Unfiltered).
2. Data were processed using an inverse filter approach with a small number (<2%) of records rejected as a result of transient detection (BLUE filter).
3. Data were taken from the Scintrex corrected file using the inbuilt noise rejecting seismic filter of an unknown type (Scintrex (seismic filtered)).

All of the processed datasets were reduced to Bouguer anomalies using standard data reduction techniques [2-4] and positional data from the total station to correct for latitude, free air effects and the effects of terrain variation. In order to provide a comparison upon which to base the efficacy of the different filtering methods, the dimensions and positions of the blocks and their density values were used in conjunction with a forward model for a parallelpiped [30] to generate the expected response. The results of this simulation and the recorded data using the different filtering regimes and the residuals in the data are shown in Figure 19. The probability density function has also been included (Figure 19c) for comparison to the instrumental errors shown in Figure 7.

Data showed limited improvements when filtered with the new technique in comparison to the inbuilt Scintrex seismic filter (RMSE = 3.87 compared to RMSE = 4.59 µGal) with similar performance for most of the measured points. However, significant improvement was observed on one of the points (point 24) which had abnormally large errors when using the Scintrex seismic filter. According to the Scintrex operating manual, the seismic filter rejects points outside of 6 standard deviations from the mean value and therefore it is possible that the method has rejected too many or too few of the points giving an erroneous final average. However, without more accurate details of the sensor's operation, it is impossible to determine the exact cause of this variation.

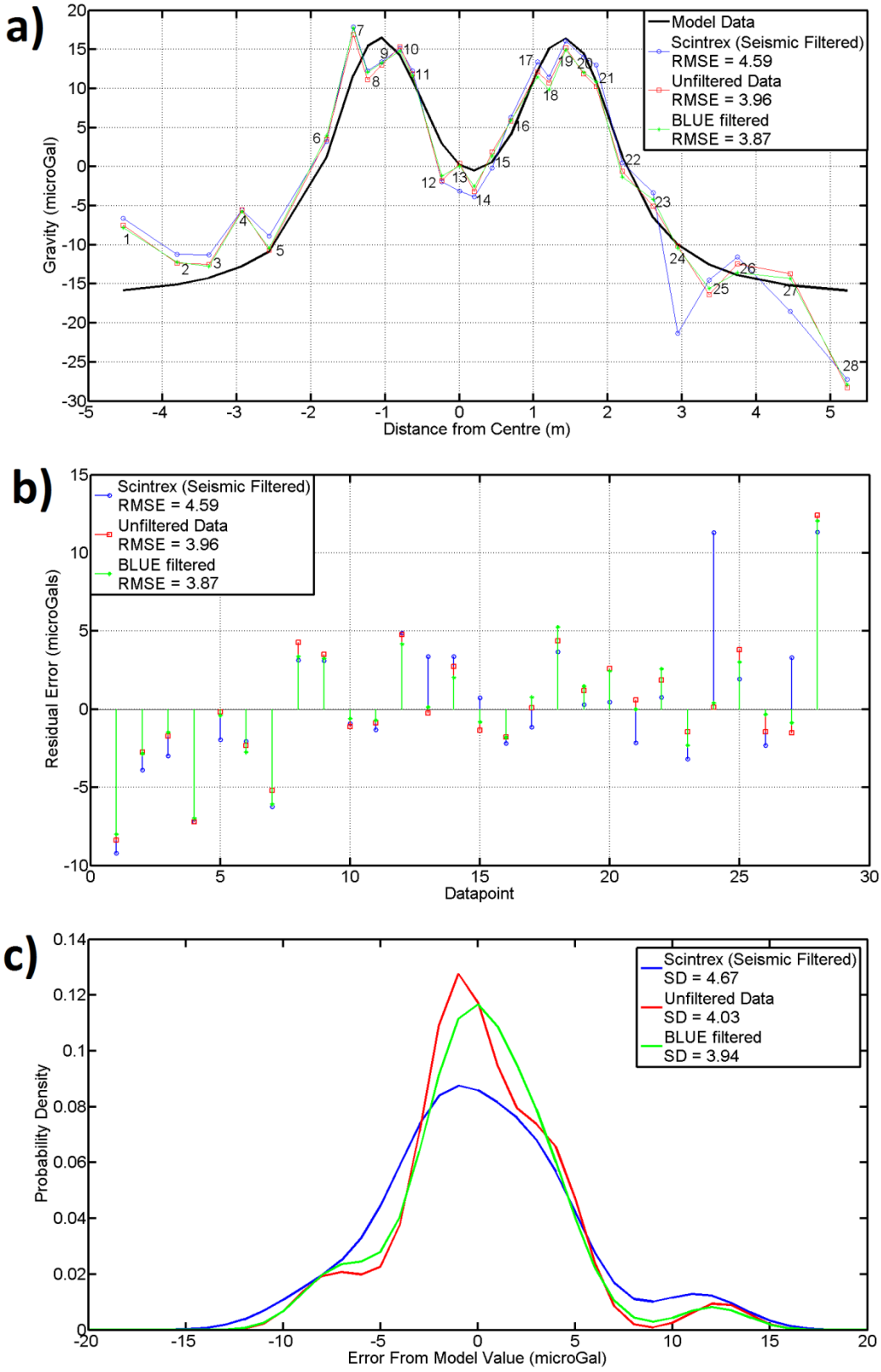

Figure 19: a) The gravity anomaly of the concrete blocks as simulated and measured using the different filtering methods and b) The point-by-point residual errors between the model data and measured data for each of the filtering methods c) The probability density functions of the errors caused by the different filtering methods

It is worth noting that since filtering showed significant improvements when the instrument was static, but not in the field data, it is clear that additional errors have been induced due to the movement of the instrument between points even though extreme care was taken to avoid shocking or tilting the instrument excessively during the survey. Since these errors are not reduced by the filtering process, it is suggested that they possess a measurement frequency longer than the instrument cycle time. Similar effects have been noted by Debeglia and Dupont [13] who noticed greater deviations between Scintrex CG3M gravimeters for several hours after using one in the field. One possibility is that the additional low frequency instrument noise comes from a physical effect on the sensor spring induced by vibrations or shocks caused by moving the instrument from point-to-point or thermal shock due to temperature variations between points [31]. However, given the low-frequency drift of the additional noise noticed by Debeglia and Dupont [13], another possibility is the long recovery time of the internal liquid tilt sensors which generates an additional drift on measurements. In either case, the limitation is the mechanical nature of the instrument and the use of a more stable instrument with no mechanical parts for field surveys such as atom interferometry sensors [32-34] will reduce these problems in the future and make the inverse filter approach invaluable in field practice in noisy environments such as urban areas. The inverse filter approach is also useful for applications using a static gravimeter or long-term sets of measurements such as in observatories, for time-lapse monitoring applications, and for base stations and reference gravity point as part of national gravity networks. In these circumstances, the inverse filter approach could provide significant benefits in terms of data acquisition time and accuracy as shown during the static measurement tests.

Conclusions

This paper has shown that gravity surveys using commercial Scintrex CG5 instruments are affected by both instrumental and environmental noise sources during measurements which greatly affect the accuracy of the collected data and have received little consideration. A long-term set of

measurements with multiple instruments was used to determine the scale of instrumental noise, which varies between instruments, and environmental noise from microseismic sources. A novel inverse filtering approach for the reduction of environmental noise was proposed, and significant improvements in the quality of microgravity data obtained in noisy conditions were shown (typically between 40% and 50% lower standard deviations). To further prove the effectiveness of the inverse filter approach, a field test was conducted over a gravity anomaly of a known size. The inverse filter approach was shown to perform marginally better than the filter in the instrument's embedded software, although the effect was negligible compared to a simple boxcar averaging process. This is thought to be due to additional noise caused by moving the instrument in field conditions which generates additional sources of noise due to effects on the spring based sensor. However, the inverse filter approach promises to greatly improve data accuracy and shorten integration times both for the next generation of instruments based on new technology such as atom interferometry and for applications involving static instruments or long occupation times using current relative gravimeter instruments resulting in cost and time savings. This will be of significant benefit to geophysical survey practitioners and will make microgravity surveys viable for many more applications.

Acknowledgements

The authors acknowledge the financial support provided by the Engineering and Physical Sciences Research Council (EPSRC) through the "Gravity Gradient Technology and Opportunities programme" EP/I036877/1.

References

1. Scintrex Ltd., *Operating Manual for the CG5 Gravity Meter*. Vol. Document Part No. 867700. 2006, Concord, Ontario: Scintrex Ltd.

2. Gabalda, G., S. Bonvalot, and R. Hipkin, *CG3TOOL: an interactive computer program to process Scintrex CG-3/3M gravity data for high-resolution applications.* Computers & Geosciences, 2003. **29**(2): p. 155-171.

3. Long, L.T. and R.D. Kaufmann, *Acquisition and Analysis of Terrestrial Gravity Data*. 2013, Cambridge: Cambridge University Press.

4. Nabighian, M.N., M.E. Ander, V.J.S. Grauch, R.O. Hansen, T.R. LaFehr, Y. Li, W.C. Pearson, J.W. Peirce, J.D. Phillips, and M.E. Ruder, *Historical Development of the Gravity Method in Exploration.* Geophysics, 2005. **70**(6): p. 63ND-89ND.

5. Seigel, H.O., *A Guide to High Precision Land Gravimeter Surveys*. 1995, Concord, Ontario: Scintrex Ltd.

6. BlÍžKovskÝ, M., *Processing and applications in microgravity surveys.* Geophysical Prospecting, 1979. **27**(4): p. 848-861.

7. Martín, A., A.B. Anquela, J. Padín, and J.L. Berné, *On standard reductions to relative gravity measurements. A case study through the establishment of the new local gravity net in the province of Valencia (Spain).* Survey Review, 2011. **43**(319): p. 16-29.

8. Charles, K. and R.G. Hipkin, *British Precise Gravity Network 1993*, in *Gravity and Geoid*, H. Sünkel and I. Marson, Editors. 1995, Springer Berlin Heidelberg. p. 39-45.

9. Camacho, A.G., J. Fernández, P.J. González, J.B. Rundle, J.F. Prieto, and A. Arjona, *Structural results for La Palma island using 3-D gravity inversion.* Journal of Geophysical Research, 2009. **114**.

10. Parseliunas, E., P. Petroskevicius, R. Birvydiene, and R. Obuchovski, *Investigation of the Automatic Gravimeters Scintrex CG-5 and Analysis of Gravimetric Measurements,.* The 8th International Conference, Vilnius, , 2011.

11. Martinez, C., Y. Li, R. Krahenbuhl, and M.A. Braga, *3D inversion of airborne gravity gradiometry data in mineral exploration: A case study in the Quadrilátero Ferrífero, Brazil.* Geophysics, 2013. **78**(1): p. B1-B11.

12. Tuckwell, G., T. Grossey, S. Owen, and P. Stearns, *The use of microgravity to detect small distributed voids and low-density ground.* Quarterly Journal of Engineering Geology and Hydrogeology, 2008. **41**: p. 371-380.

13. Debeglia, N. and F. Dupont, *Some critical factors for engineering and environmental microgravity investigations.* Journal of Applied Geophysics, 2002. **50**(4): p. 435-454.

14. Bonvalot, S., M. Diament, and G. Gabalda, *Continuous gravity recording with Scintrex CG-3M meters:a promising tool for monitoring active zones.* Geophysical Journal International, 1998. **135**(2): p. 470-494.

15. Lederer, M., *Accuracy of the relative gravity measurement.* Acta Geodyn Geomater, 2009. **6**: p. 383-390.

16. Reudink, R., R. Klees, O. Francis, J. Kusche, R. Schlesinger, A. Shabanloui, N. Sneeuw, and L. Timmen, *High tilt susceptibility of the Scintrex CG-5 relative gravimeters.* J Geod, 2014. **88**: p. 617-622.

17. Liard, J., G. Carey, D.B. Hearty, P. Salib, and T.R. Flint, *Evaluation of the Scintrex CG-3 gravity meter.* Geological Survey of Canada Open File Report 1993. **2696**.

18. Jiang, Z., V. Pálinkáš, O. Francis, P. Jousset, J. Mäkinen, S. Merlet, M. Becker, A. Coulomb, K.U. Kessler-Schulz, H.R. Schulz, R. Ch, L. Tisserand, and D. Lequin, *Relative Gravity Measurement Campaign during the 8th International Comparison of Absolute Gravimeters (2009).* Metrologia, 2012. **49**(1): p. 95.

19. Ardhuin, F., E. Stutzmann, M. Schimmel, and A. Mangeney, *Ocean wave sources of seismic noise.* Journal of Geophysical Research - Oceans, 2011. **116**: p. C09004.

20. Essen, H.H., F. Krüger, T. Dahm, and I. Grevemeyer, *On the generation of secondary microseisms observed in northern and central Europe.* Journal of Geophysical Research: Solid Earth, 2003. **108**(B10): p. 2506-2520.

21. Allis, R.G., P. Gettings, and D.S. Chapman, *Precise Gravimetry and Geothermal Reservoir Management.* Proceedings of the Twenty-Fifth Stanford Workshop on Geothermal Reservoir Engineering, 2000: p. 179-188.

22. Sugihara, M., *Gravity monitoring with a CG5 Scintrex autogravimeter.* ASEG Extended Abstracts, 2004. **2004**(1): p. 1-4.

23. Goodkind, J.M., *Continuous measurement of nontidal variations of gravity.* Journal of Geophysical Research: Solid Earth, 1986. **91**(B9): p. 9125-9134.

24. Longman, I.M., *Formulas for Computing the Tidal Accelerations Due to the Moon and the Sun.* Journal of Geophysical Research, 1959. **64**(12): p. 2351-2355.

25. Matsumoto, K., M. Ooe, T. Sato, and J. Segawa, *Ocean tide model obtained from TOPEX/POSEIDON altimetry data.* J. Geophys. Res, 1995. **100(C12)**(25): p. 319-330.

26. Pfeiffer, T. *Volcano Discovery*. 2015 [cited 25/11/15]; Available from: http://www.volcanodiscovery.com/earthquakes/archive/2015-jun.html.

27. Isotalo, J., S. Puntanen, and G.P.H. Styan, *The BLUE's covariance matrix revisited: A review.* Journal of Statistical Planning and Inference, 2008. **138**(9): p. 2722-2737.

28. Rao, C.R. *Least squares theory using an estimated dispersion matrix and its application to measurement of signals*. in *Proceedings of the Fifth Berkeley Symposium on Mathematical Statistics and Probability, Volume 1: Statistics*. 1967. Berkeley, Calif.: University of California Press.

29. Hassanpour, H., M. Mesbah, and B. Boashash, *EEG spike detection using time-frequency signal analysis*, in *Proceedings of the IEEE International Conference on Acoustics, Speech, and Signal Processing, 2004 (ICASSP '04). Vol. 5*. 2004, IEEE: Montreal, Canada. p. 421-424.

30. Telford, W.M., L.P. Geldart, and R.E. Sheriff, *Applied Geophysics*. 2nd Edition ed. 1990, Cambridge: Cambridge University Press.

31. Yushkin, V.D., *Operating experience with CG5 gravimeters.* Measurement Techniques, 2011. **54**(5): p. 486-489.

32. Freier, C., M. Hauth, V. Schkolnik, B. Leykauf, M. Schilling, H. Wziontek, H.G. Scherneck, J. Müller, and A. Peters, *Mobile quantum gravity sensor with unprecedented stability.* Journal of Physics: Conference Series, 2016. **723**(1): p. 012050.

33. Peters, A., K.Y. Chung, and S. Chu, *High-precision gravity measurements using atom interferometry.* Metrologia, 2001. **38**(1): p. 25.

34. Peters, A., K.Y. Chung, and S. Chu, *Measurement of gravitational acceleration by dropping atoms.* Nature, 1999. **400**(6747): p. 849-852.

Figures

Figure 1: 30 second sections of longer gravity measurements showing the effect of measurement high-frequency noise. Notice the imbalance in positive and negative fluctuations around the mean (defined as zero). a) Microseism noise only b) microseism and wind noise spikes with negative spikes c) microseism and road traffic noise with positive spikes d) microseism and earthquake noise introducing a low-frequency signal which dominates the microseism noise

Figure 2: The three instruments used to characterise the noise in the basement in the University of Birmingham

Figure 3: Examples of the different corrections applied to the gravity data a) temperature correction b) tilt correction c) Celestial tidal correction d) ocean tidal loading correction and e) drift correction. The effects of these different corrections on raw gravity data are also shown f) No corrections g) Temperature corrected h) Temperature and tilt corrected i) Temperature, tilt corrections and celestial tidal model applied j) Temperature, tilt corrections and celestial and ocean tidal models applied k) Temperature, tilt corrections and celestial and ocean tidal models applied then corrected for drift using linear trend.

Figure 4: The residual tidal signal after data processing steps shown in figure 3 and removal with a polynomial fit

Figure 5: FFT analysis of 37.5 hours of data collected using 3 Scintrex CG5 instruments simultaneously. Peaks at similar frequencies are shown within the measurement cycle but the instrument noise predominantly affects the lower frequencies

Figure 6: a) The error of the mean on individual 256 second measurements representing the efficacy of the averaging process on removing environmental noise and b) the actual errors of the measurements from the three instruments

Figure 7: Probability density function of instrumental errors expressed as deviation from the mean value after all environmental signals have been removed

Figure 8: The overlapping Allan Deviation of the long period measurements

Tables

Highlights

- Microgravity instrumental and environmental noise sources are assessed and quantified
- Digital filter is proposed for eliminating environmental sources of noise
- Significant improvement of 40-50% were found in test conditions
- Additional source of noise from moving the instrument during surveying is identified
- Filter will speed up and increase accuracy with future atom interferometry instruments